

Cite this: *Inorg. Chem. Front.*,

2017, 4, 595

Received 31st October 2016,

Accepted 22nd December 2016

DOI: 10.1039/c6qi00468g

Hybrid molecular-inorganic materials: Heterometallic [Ni₄Tb] complex grafted on superparamagnetic iron oxide nanoparticles

L. Rosado Piquer,^a E. Jiménez Romero,^c Y. Lan,^b W. Wernsdorfer,^{b,d} G. Aromí,^a E. C. Sañudo^{a,*}

A heterometallic Ni₄Tb field-induced SMM has been grafted onto the surface of superparamagnetic iron oxide nanoparticles. The magnetic coupling within the Ni₄Tb and between the Ni₄Tb and iron oxide nanoparticle has been studied by element specific XMCD measurements. The coupling between Ni and Tb is ferromagnetic and the complex remains intact when grafted onto the iron oxide nanoparticles.

Introduction

The topic of nanostructured materials that combine a magnetic or metallic surface with a molecule is on the spotlight due to the implications of this research in the implementation of molecular spintronics,^{1–3} or the use of molecules for information processing or storage.^{4–7} In this area, it becomes increasingly important to understand and if possible control the interaction of the molecule with the surface it is deposited on, since for any possible application we can envision using single molecule magnets (SMMs) or molecular nanomagnets (MNMs) an unavoidable step will be to graft the molecules on a surface.⁸ The substrate might be the surface of a simple break-junction electrode^{9,10} or a multi-layered substrate. In this study we have chosen iron oxide as the substrate, prepared in the form of iron oxide nanoparticles decorated with dopamine. The preparation and characterization of iron oxide magnetic nanoparticles (NP) has been a very active field of research for the last couple of decades. Precise synthetic methods have been developed since their discovery and now they can be readily prepared.^{11,12} Iron oxide NP have many potential applications in fields as diverse as magnetic information storage,¹³ nanomedicine^{14,15} or catalysis.^{16–18} One of the main features of iron oxide NP is the fact that they can be easily separated using a magnetic field. This has fostered the use of iron oxide NP as 'carriers' of other molecules that can be deposited on their surface. One example is the magnetic removal of catalysts from a homogenous medium as reported by Bronstein and co-workers, among others.¹⁶ In this paper we use well-known iron oxide nanoparticles as the support for a hybrid material containing a 3d-4f molecular nanomagnet. The system is ideal, since it is easy to manipulate in solution and it is a good model for a magnetic surface. Furthermore, the iron oxide NP used in this study are decorated with dopamine. This is key to address the decoupling of the SMM to the surface. It has become an

increasing concern among researchers that SMMs and MNMs directly deposited on a magnetic surface, as needed for spintronic applications, will have their molecular properties greatly affected by coupling with the surface. This leads to the lack of hysteresis loops for SMMs on surfaces, which have only been observed at very low temperatures for Fe₄ on Au¹⁹ or TbPc SMM on HOPG,²⁰ both non-magnetic substrates. Recently, Dreiser and co-workers have successfully measured hysteresis loops for TbPc SMM on Ag, a non-magnetic substrate, by decoupling the SMM from the surface using MgO.²¹

Microwave assisted synthesis has been applied in the last few years by groups like Brechin and co-workers^{22,23} and ours^{24–26} to the synthesis of polynuclear coordination complexes with very exciting results. In a way, microwave assisted synthesis is similar to solvothermal synthesis²⁷ but reaction times are much shorter (of the order of minutes). We have also been interested in using solvent-free reactions in coordination chemistry.^{28,29} In this type of synthesis, the ligands and metal salts are heated up to a melt, from which a coordination chemistry complex can be extracted using organic solvents. We have extended this to microwave assisted synthesis with several advantages: the reactions are very fast (10 minutes or less) thus the energy consumption is small, very small amounts of organic solvents are used on the extraction (5 mL or less) so chemical waste is reduced to a minimum and pure products can be obtained in crystalline form.

X-ray Magnetic Circular Dichroism (XMCD) has proven to be an excellent and very powerful technique to characterize heterometallic complexes since it allows the measurement element specific magnetization curves.³⁰ The sensitivity of XMCD along with the possibility of being element specific make it ideal to characterize molecules on surfaces since the signal from a substrate can be easily ignored.^{31–34,35} This is particularly relevant when the substrates are magnetic, as proposed for spintronic applications.

We report here the first use of melt microwave assisted reaction applied to 3d-4f complexes. Reports of 3d-4f SMMs have increased exponentially since 2004,³⁶ when the first 3d-4f SMMs were reported. The interest in new 3d-4f complexes as promising materials for new applications like molecular spintronics, magnetic cooling or information storage and processing is ever growing. However, ways of forming monolayers of molecular species on surfaces or nanostructured materials with molecular species is still a challenge. We present here the synthesis of the field-induced SMM $[\text{Ni}_4\text{Tb}(\text{OH})_2(\text{chp})_4(\text{tBuSALOH})_5(\text{H}_2\text{O})(\text{MeCN})(\text{MeOH})]$ (Ni_4Tb) (chp = 6-chloro-2-hydroxypyridine, tBu-SALOH = 3,5-ditertbutylsalicylato), along with its characterization in bulk and we report a hybrid system characterized by element specific magnetization curves.

Results and Discussion

Ligands with low melting points (i.e. below 200 °C, 473 K) are ideal candidates for solvent free reactions in a microwave reactor. In this paper we report the results obtained with 6-chloro-2-hydroxypyridine (chp, melting point 128-130 °C) and 3-5-ditertbutylsalicylic acid (tBu-SALOH, melting point 157-162 °C). Freshly prepared nickel hydroxide and hydrated terbium (III) acetate with the ligands were ground in a mortar and introduced in the microwave reactor cavity. Microwave pulses of different intensities were scanned and the 300 W pulse was chosen, since it produced the best yield of product. The grinding of the reagents helps in the homogenization of the reaction mixture but it is not a determinant factor in the yield. Reactions without grinding produced comparable yields. Upon application of a microwave pulse temperature was controlled so that the organic reagents melt. Once the reaction was cooled a green solid was obtained. The IR spectrum of the solid was very similar to that of the product $[\text{Ni}_4\text{Tb}(\text{OH})_2(\text{chp})_4(\text{tBuSALOH})_5(\text{H}_2\text{O})(\text{MeCN})(\text{MeOH})]$ (Ni_4Tb). This is a clear indication that the tBu-SALO and chp ligands are already coordinated to the Ni(II) and Tb(III) ions. The solid was extracted with the minimum amount of MeOH/MeCN mixture (1:1 in volume) and the green solution obtained was left undisturbed. Green crystals suitable for single crystal X-Ray diffraction were obtained after several days. Analogous bench-top reactions were tested but Ni_4Tb was not obtained. A lanthanum analogue that contains no unpaired *f* electrons was prepared to help us understand the magnetic properties of Ni_4Tb . The synthesis proceeded exactly as that of Ni_4Tb but with a lower yield.

Ni_4Tb is an ideal candidate for our aims since it contains Ni and Tb and the two metals have terminal solvent ligands, some of which will be easily replaced by/or form hydrogen bonds to the NH_2 terminal groups of dopamine. Furthermore, the heterometallic nature of Ni_4Tb will facilitate the study of the magnetic coupling in the complex in the bulk and on the surface of a substrate, in this paper a superparamagnetic nanoparticle, by element specific magnetization curves.

Crystal structure of Ni_4Tb

Scheme 1

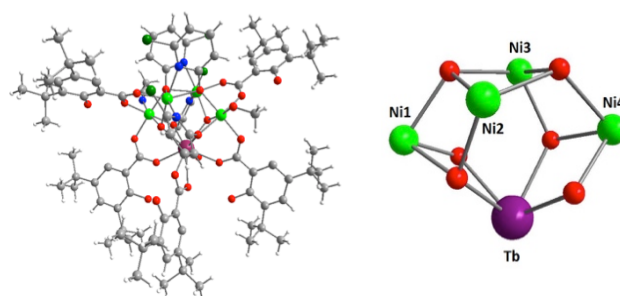
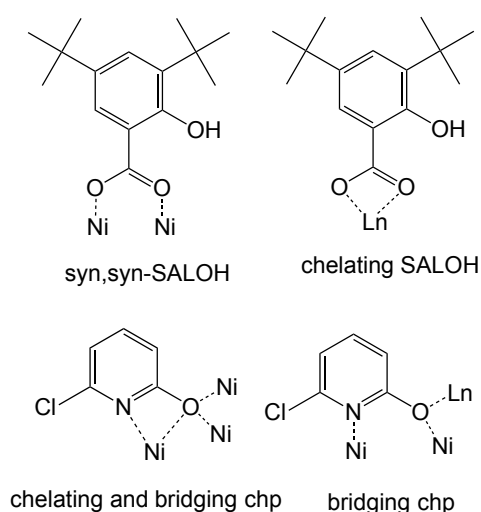


Figure 1. Labeled core and crystal structure of Ni_4Tb . Ni atoms in light green, Tb in purple, oxygen in red, nitrogen in blue, carbon in gray, chlorine in green and hydrogen in white (colour online).

Table S1 in the supplementary material contains the crystallographic data and structural parameters for complexes Ni_4Tb and Ni_4La . The lanthanum analogue is isostructural to Ni_4Tb and only the latter will be discussed here. Ni_4Tb crystallizes in the monoclinic space group $P2_1/c$. The asymmetric unit contains the whole molecule and non-coordinated solvent molecules. The crystal structure and the core of Ni_4Tb are shown in Fig. 1. The core consists of one Tb(III) ion linked to four Ni(II) ions by oxygen bridging ligands, two of these oxygens are provided by μ_3 -hydroxo groups and the other four are from deprotonated chp ligands. Scheme 1 shows the observed coordination modes for the chp and tBu-SALOH ligands. There are four tBu-SALOH ligands bridging every Ni(II) ion to the Tb(III) ion in the typical *syn,syn* bridging mode of carboxylato ligands, where the OH group of the salicylato is not used. The other tBu-SALOH ligand is chelating the Tb(III). Two chp ligands are bridging three metals and chelating one metal using the oxygen and nitrogen donors. The two remaining chp ligands are bridging the Tb(III) ion to Ni1 and Ni4. The four Ni(II) ions are hexacoordinated with distorted octahedral geometries. The Tb(III) ion is ennea-coordinated with a distorted geometry closer to a spherical tricapped trigonal prism. To complete its coordination sphere,

Ni1 ion is bonded to one terminal MeOH molecule, Ni4 is bonded to one terminal MeCN molecule and the Tb(III) ion is bonded to one terminal water. These terminal solvent ligands are the grafting points for the attachment of the complex to the NP. The number of 3d-4f complexes reported has been growing exponentially, as we pointed out in our review on the topic of 3d-4f SMMs.³⁷ There are very few intermolecular interactions in the crystal packing of Ni₄Ln, limited to weak Van der Waals interactions between tert-butyl groups of the tBu-SALO ligands. There are 434 crystal structures reported on the Cambridge Crystallographic Database that contain Ni(II) and one of the lanthanide ions, these include molecular as well as polymeric structures. However there is only one report of a [Ni₄Ln] complex (Ln = Gd, Tb, Dy, Ho) by Chandrasekhar and co-workers.³⁸ The structure of the complexes reported by Chandrasekhar can be best described as two [Ni₂] units linked by a central lanthanide ion and it is completely different to the core of the complexes reported here. Thus, Ni₄Tb and Ni₄La are new structural types in the growing family of 3d-4f complexes.

Magnetic properties of Ni₄Tb

Magnetic susceptibility data were collected for the Ni₄Tb complex in the 2-300 K temperature range at an applied field of 3000 Oe. Additional data were collected below 25 K at a field of 300 Oe. No field dependence was observed. The data are shown in Figure 2 as a χT vs. T plot. The χT product value at 300 K is in agreement with the expected value for four Ni(II) ions ($g = 2.2$, $S = 1$) and one terbium (III) ion (7F_6 , $S = 3$, $L = 3$, $J = 6$ and $g_J = 3/2$). As temperature decreases the χT product remains nearly constant until an increase is observed below 50 K indicating the population of a ferromagnetically coupled spin ground state. Thus, the magnetic interaction in the complex is ferromagnetic. This increase was also observed in the lanthanum analogue of the complex, thus in the absence of 4f unpaired electrons the four Ni(II) centres are also ferromagnetically coupled. The susceptibility data of Ni₄La, was subtracted from the data for Ni₄Tb. The curve obtained was not that of an isolated Tb(III) ion, as can be seen in Figure 2, an increase is observed as temperature decreases indicating that there is in fact ferromagnetic coupling between Ni and Tb in Ni₄Tb. Four Ni-O-Tb angles are between 101-104° and two Ni-O-Tb angles are 120° and 121°, the Ni-O-Ni angles are all between 92-98°, except the 116-117° formed between Ni-O-chp-Ni, so predominant ferromagnetic coupling is expected.³⁹ The magnetic data for Ni₄La were fitted simultaneously using a two-J model with the software PHI.⁴⁰ The Hamiltonian used by the program is $\hat{H} = \hat{H}_{ANIS} + \hat{H}_{EX} + \hat{H}_{Zeeman}$ where Stevens operators are used for the anisotropy and the exchange Hamiltonian is $\hat{H}_{EX} = -2 \sum J_i \hat{S}_i \cdot \hat{S}_j$. The coupling between the Ni(II) ions is ferromagnetic. The best fitting for susceptibility and magnetization are shown in Figures 2 and 3 as solid lines. The best fitting parameters with a g value of 2.26 were $J(23) = J(12) = J(34) = +1.18 \text{ cm}^{-1}$ and $J(13) = J(24) = +1.23 \text{ cm}^{-1}$ with the Ni(II) ions numbered as in Figure 1. The D values were $D(1)=D(4) = 18.60 \text{ cm}^{-1}$ and $D(2)=D(3) = 4.04 \text{ cm}^{-1}$. The positive anisotropy of the Ni(II) ions is in agreement with the fact that Ni₄La is not an SMM.

In order to check if Ni₄Tb is a new example of 3d-4f SMMs, dynamic ac magnetic susceptibility data were collected between 30 K and 1.8 K. The data showed the absence of out-of-phase signals for Ni₄Tb.

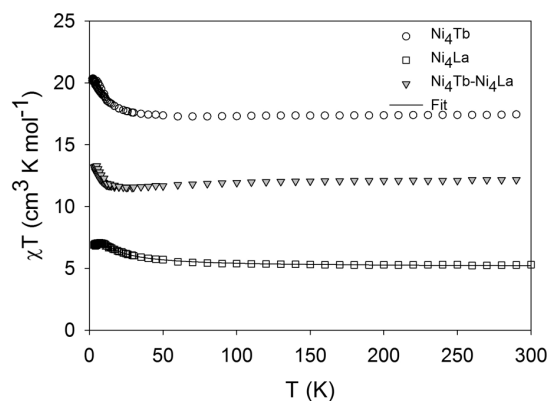


Figure 2. Magnetic susceptibility for Ni₄Tb (circles) and Ni₄La (squares) shown as χT vs. T plots. Susceptibility of Ni₄Tb minus susceptibility of Ni₄La is shown as triangles.

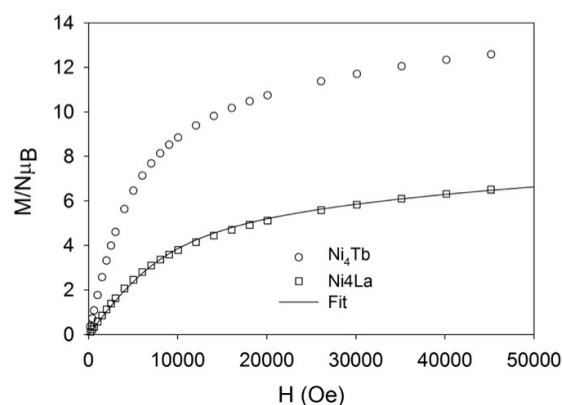


Figure 3. Magnetization vs. field data collected at 2 K plot for Ni₄Tb (circles) and Ni₄La (squares).

Data were also collected at 100 and 1000 Hz with various applied magnetic fields between 1000 Oe and 2500 Oe. At 100 Hz, the tail of an out-of-phase signal clearly appears below 5 K (see Figure S2). The signal corresponds to a fast dynamic relaxation process probably due to quantum tunneling of the magnetization that is partially quenched by the application of a magnetic field.

Magnetization hysteresis loops were collected in the mK temperature range on a single crystal of Ni₄Tb using a microSQUID (see supplementary material Figure S3). The quantum tunneling effect leads to a closed hysteresis loop at zero dc field and with the increase of field a temperature- and sweep rate-dependent hysteresis loop opens up below 0.5 K. Thus Ni₄Tb is a new example of field-induced SMM behavior. Ni₄Tb does not display hysteresis of the magnetization at 2 K. Dynamic ac magnetic susceptibility data were also collected for Ni₄La. There is no evidence of slow relaxation down to 2 K with and without applied magnetic fields, so Ni₄La is not an SMM.

The slow relaxation properties of Ni_4Tb are thus related to the presence of Tb(III) and/or the Tb-Ni magnetic coupling. The magnetic properties of the complexes reported here are similar to those reported for $[\text{Ni}_2]_2\text{Tb}$ reported by Chandrasekhar and coworkers,³⁸ where they also observe weak ferromagnetic coupling. This fact is due to the coincidence on the Ni-O-Ni angles that lead to ferromagnetic coupling but not to a structural similarity beyond the Ni-O-Ni angles. However, Chandrasekhar and co-workers do not report any SMM properties for their 3d-4f complexes.

Decoration of NP with Ni_4Tb (NP- Ni_4Tb) and characterization of the hybrid system

Scheme 1

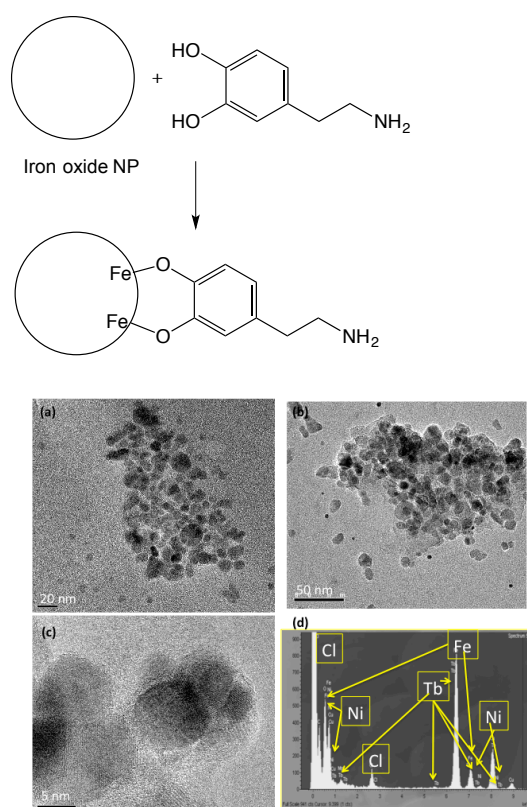


Figure 4. TEM images of dopamine functionalized NP (a); loaded NP- Ni_4Tb (b) and (c); EDX spectrum of NP- Ni_4Tb with the Cl, Ni, Tb and Fe peaks highlighted (d).

In order to prepare hybrid systems with iron oxide nanoparticles and Ni_4Tb we have chosen a reported synthesis for the nanoparticles functionalized with dopamine.^{17,18} This synthesis is well known and produces magnetic iron oxide nanoparticles of relatively low size-dispersion that expose the NH_2 groups of dopamine (Scheme 1).

The resulting material consisted of circa. $9.8 \pm 21\%$ nm crystalline NP with exposed NH_2 donor groups that make these amenable to further functionalization by coordination to other metals or complexes that have available coordination sites or hydrogen bonding sites like a coordinated water molecule. This method was chosen over other methods because it provides NP that are not coated with a surfactant like oleic acid, since ligand exchange once NP are coated by i.e. oleic acid is not

trivial¹⁶. The NP were characterized by TEM, as shown in Figure 4, they are crystalline and agglomerate easily.

The obtained material are aggregates of crystalline superparamagnetic nanoparticles of mixed valent Fe(II)/Fe(III) oxide with an inverted spinel structure, some oxidation to Fe_2O_3 may occur in such small NP, as reported by Park et al, and solid solutions of $\text{Fe}_2\text{O}_3/\text{Fe}_3\text{O}_4$ are obtained.¹² The nanoparticles are magnetized at room temperature. After magnetic separation of the NP functionalized with dopamine, these were dispersed in MeOH and sonicated. Ni_4Tb was added to the solution and the sample shaken for several hours to allow grafting of Ni_4Tb . The resulting material was separated by decantation using a hard magnet and the solid was washed several times to ensure that there were no traces of unattached Ni_4Tb . The solid was re-dispersed in MeOH in order to study its morphology and composition by TEM and for dynamic light scattering studies (DLS). DLS data on the dopamine functionalized NP showed a broad distribution of dynamic radius in MeOH solution; the DLS radius observed was 30-50 nm, larger than the NP diameter observed by TEM, as expected due to aggregation facilitated by the terminal NH_2 groups of dopamine. The iron oxide NP loaded with Ni_4Tb had dynamic radius of 90-100 nm in MeOH solution at similar concentration showing that aggregates are formed in a more controlled fashion with the hydrophobic surface exposed by the Ni_4Tb complexes that load the NP. The analysis of the particle size distribution using the TEM images of NP- Ni_4Tb showed that the loaded NP- Ni_4Tb size distribution is $9.2 \pm 21\%$ nm, very similar to that of the unloaded NP sample and the NP- Ni_4Tb are crystalline. Furthermore, the decoration with Ni_4Tb exposes a hydrophobic surface, with exposed *tert*-butyl groups that favor further aggregation of the NP by weak C-H...C-H interactions.⁴¹ The hybrid system NP- Ni_4Tb is also magnetized at room temperature.

Energy dispersive X-ray analysis (EDX) performed on the pristine NP and on the decorated NP- Ni_4Tb showed the presence of Ni and Cl in the samples loaded with Ni_4Tb , as expected. The amount of Tb was in the expected ratio compared to the amount of Ni (one Tb per four Ni ions). However, the peaks of Tb in the EDX spectrum are very close to the Fe peaks, so even if EDX seems to suggest the presence of Tb it is not conclusive. The Tb content is confirmed by XMCD Tb-edge specific magnetic data and XAS.

Magnetic characterization of the hybrid system NP- Ni_4Tb

Magnetization vs. field data at 2 K were collected for the dopamine functionalized NP and the hybrid NP- Ni_4Tb . The data are presented in Figure 5 as magnetization per gram of material vs. field. Clearly, the NP magnetism dominates the bulk data. There is a 3% reduction in the saturation magnetization at 5 T for the NP- Ni_4Tb material with respect to the dopamine functionalized NP. This indicates that circa. 4-8 % w/w of the sample is Ni_4Tb . This value is in agreement with a rough estimate of the number of Ni_4Tb molecules covering the surface of a NP of approximately 5-6 nm radius. The coercive field of the hysteresis loop at 2 K for the dopamine functionalized NP was 331 Oe, while the coercive field

measured at zero field cool (ZFC) and 2 K for the hybrid NP-Ni₄Tb material was enhanced to -399 Oe and 350 Oe, shifted to negative fields. Hysteresis cycles were measured at different field cool magnetic fields (0.2 T, HE = 48 Oe; 0.5 T, HE = 32 Oe and 5.0 T, HE = 17 Oe). They all showed a exchange bias fields (HE) that shifts to more positive values as the FC field is increased (see Supplementary Material, Figure S5), this kind of horizontal shift in the hysteresis loops is usually attributed to antiferromagnetic coupling. In this case the values are too small to affirm that there is a clear interaction between the NP and the Ni₄Tb shell mediated by the dopamine that decorates the iron oxide NP.^{42–44}

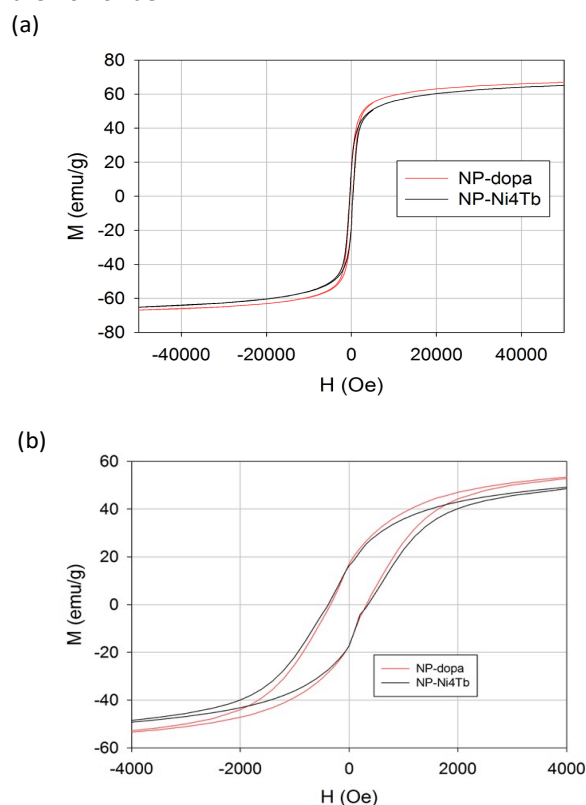


Figure 5. (a) Magnetization vs. field hysteresis loops at 2 K for the dopamine functionalized iron oxide NP (red line) and the hybrid material NP-Ni₄Tb (black line). (b) Zoom of the -4000 to 4000 Oe region.

Exchange bias has been observed in core-shell NP,⁴³ in coupled aggregates of SMMs^{45,46} or on SMMs coupled to a magnetic surface^{47,48} additionally to the seminal studies on biasing on heteromagnetic multilayers.^{42,49,50} SQUID magnetometry can be used to study the hybrid NP-SMM system but the data that can be obtained is clearly dominated by the magnetic substrate, the iron oxide NP, thus it is very difficult, if not impossible to extract conclusions as to the coupling between NP and Ni₄Tb via the dopamine linker.

XMCD studies of Ni₄Tb and NP-Ni₄Tb

Heterometallic complexes are particularly amenable to XMCD studies. Dreiser and co-workers reported in 2012 the use of XMCD in order to address the 3d-4f magnetic interaction in a heterometallic complex.³⁰ In order to study the magnetic

coupling between Ni(II) and Tb, X-ray Magnetic Circular Dichroism is a great technique that allows the study of the magnetization of two elements in the same complex.

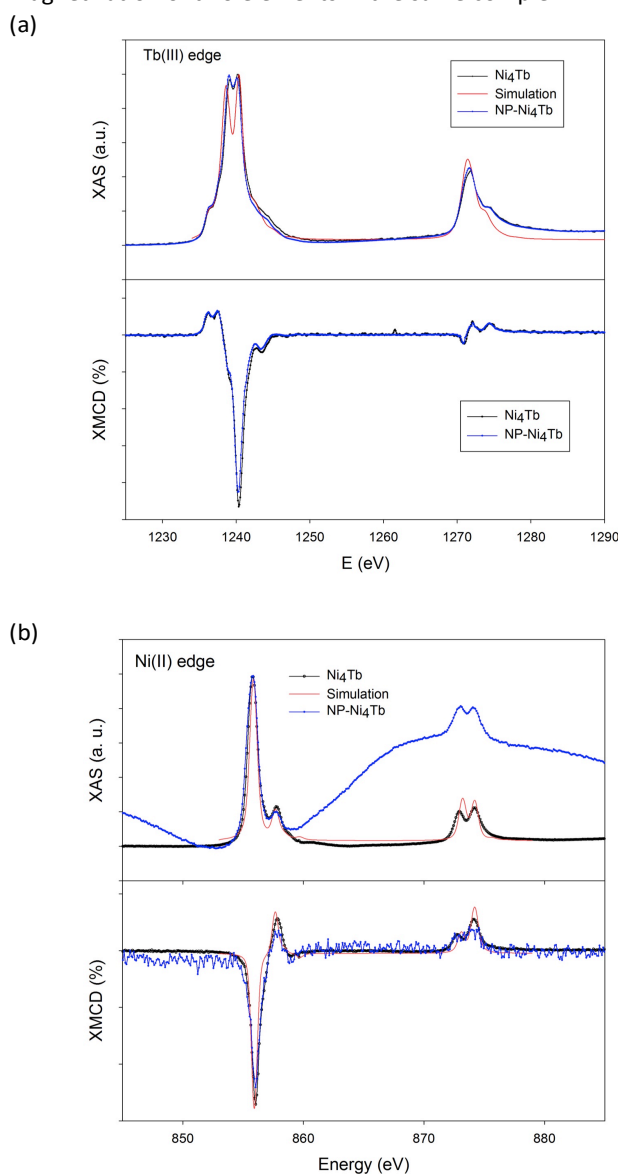


Figure 6. Normalized XAS at the L_{2,3} edges of Ni and at the M_{4,5} edges of Tb with positive and negative circular polarization and X-ray magnetic circular dichroism spectra of Ni₄Tb and NP-Ni₄Tb at Tb-edge (top.) and Ni-edge (bottom) collected at the lowest temperature (aprox. 7 K) and 5 T. The data for the NP-Ni₄Tb system are normalized to be in the same scale. The red lines are simulations performed with the graphic version of CT4MXAS software.

The magnetic coupling between Ni and Tb in pure Ni₄Tb was studied by XMCD at ID-32 at ESRF, with a superconducting coil applying magnetic fields up to the maximum field of 9 T, when the cryostat temperature was 5 K. The sample temperature in this set-up is slightly higher than the cryostat temperature. The lowest temperature was reached by cooling with liquid helium (T = 4 K) while the real temperature at the sample was approximately 7 K limited by the quality of the thermal contact in this set-up. Measurements were performed on a pure sample of Ni₄Tb. X-ray absorption data were collected at the

$L_{2,3}$ edges of Ni and at the $M_{4,5}$ edges of Tb with positive ($I+$) and negative ($I-$) circular polarization of the light.

The XMCD signal was calculated as the difference between XAS spectra at positive ($I+$) and negative ($I-$) circular polarization recorded in a magnetic field. A negative L_3 or M_5 peak is expected if the magnetic moment is parallel to the applied magnetic field. Total electron yield (TEY) was used as detection technique. The data are shown in Figure 6 as Ni and Tb XAS and dichroic spectra. For Ni(II) the XAS spectrum, represented as the average value between positive and negative circularly polarized light XAS, shows the promotion of an electron from the $2p^6$ core shell to the $3d^8$ valence shell, with the final state being $2p^5 3d^9$. The $2p$ - $3d$ absorption spectrum is characterized by two distinct absorption bands (L_3 and L_2) with distinct features directly related to the crystal field around the Ni(II) ions. For Tb(III) the XAS spectra is related to the transition from $3d^{10} 4f^8$ to $3d^9 4f^9$. The core shell is now $3d$ and the valence shell is $4f$. The $3d$ - $4f$ absorption spectrum for Tb(III) is characterized by two features (M_5 and M_4) clearly separated in energy. The data clearly show that Ni(II) and Tb(III) have their spins parallel and parallel to the applied magnetic field. The element specific magnetization curves (see Supplementary Material, Figure S06) support the ferromagnetic coupling observed by SQUID magnetometry results.

The experimental XAS and XMCD spectra were used to calculate the effective magnetic moment in both Ni and Tb in Ni_4Tb considering the dipolar transition rules for Ni and Tb that allow one to calculate the expectation values of the projection of the orbital $\langle L_z \rangle$ and spin moments $\langle S_z \rangle$, which in turn can be used to obtain the effective moment, m_z (in Bohr magnetons).⁵¹ For the transition metal, $\langle S_z \rangle$ can be approximated to the effective spin value, S_{eff} .⁵² The values obtained for Tb in Ni_4Tb are $\langle S_z \rangle = -1.15$, $\langle L_z \rangle = -1.54$ and $m_z = 3.84 \mu_B$. This value is lower than the expected ones for a free Tb(III) ion with a Hund's rule ground state $J = 6$, $S = 3$ and $L = 3$ and a theoretical saturation moment of $9 \mu_B$. This large difference is due to the crystal field and the magnetic coupling, even if the crystal field is a small factor for lanthanide complexes it cannot be neglected: in Ni_4Tb the Tb is not behaving as a free ion but is coupled to the rest of the molecule. For Ni(II) in Ni_4Tb the values obtained are $\langle S_z \rangle = S_{\text{eff}} = -1.37$, $\langle L_z \rangle = -0.53$ and $m_z = 3.28 \mu_B$. The values are in agreement with the expected for a Ni(II) ion in a crystal field, that is $S_{\text{eff}} = 1$ and effective moment of $2.82 \mu_B$. Furthermore, as expected from the visual analysis of the XMCD spectra, the magnetic moments of Tb and Ni have the same sign and are parallel. The XAS spectra of Ni and Tb were simulated using CTM4XAS software (<http://www.anorg.chem.uu.nl/CTM4XAS/>) taking into account spin-orbit coupling and crystal field for Ni(II). The simulations are shown in Figure 6 as red lines. They fit reasonably well both the XAS spectra of the Ni_4Tb complex and the XAS spectra obtained from NP- Ni_4Tb system. The available version with a graphic user interface of the software does not allow introduction of crystal field for lanthanide ions, so XMCD spectra for Tb was not be calculated.

XAS spectra at positive and negatively polarized light were measured for NP- Ni_4Tb sample at the Ni, Tb and Fe edges. The

data obtained could answer the two very relevant questions of whether the molecule is intact in the nanostructured system and whether it is coupled to the magnetic support. This is key information for understanding the coupling of a molecule to a ferromagnetic surface or electrode, which in turn is a very important point to address for the development of spintronic devices based on molecular nanomagnets. In this respect, the choice of an heterometallic complex is not trivial: we have selected Ni_4Tb for this study since it allows us to study the element specific magnetism of Fe from the NP and Tb and Ni from the complex. This should enable us to establish without ambiguities that Ni_4Tb is intact on the NP surface.

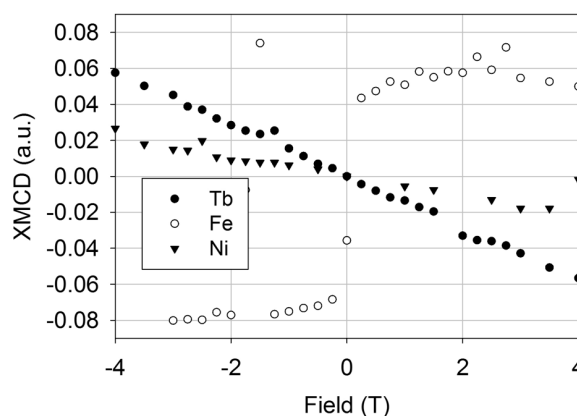


Figure 7. Element specific magnetization vs. field loops at 5 K for NP- Ni_4Tb : Ni, Tb in blue (stars and circles) and Fe in black squares (709 eV peak).

XAS data at the $L_{2,3}$ edges of Fe and Ni and at the $M_{4,5}$ edges of Tb with positive ($I+$) and negative ($I-$) circular polarization of the light were collected for the hybrid NP- Ni_4Tb system at circa. 7 K. The XMCD signal was calculated as the difference between XAS spectra at positive ($I+$) and negative ($I-$) circular polarization recorded in a magnetic field of 5 T at TEY. At this field with the lowest temperature available in the set-up the Ni and Tb signals are not saturated but the Fe signal of the NP is completely saturated. At the sample temperature of approx. 7 K and 5 T the magnetization of pure Ni_4Tb is 84% of the value of the magnetization at 2 K (see supplementary information Figure S2) and it is paramagnetic. The data collected for the hybrid NP- Ni_4Tb system are shown in Figure 6 as XAS and XMCD spectra at Ni and Tb-edges and in Figure 7 as Fe, Ni and Tb magnetization curves. They clearly show a paramagnetic behavior for Ni and Tb similar to that observed for Ni_4Tb in SQUID measurements at 8 K (see supplementary information Figure S2), with their spins parallel. The data for Ni in the NP- Ni_4Tb system is less intense than for the pure complex, as expected due the low w/w % of Ni_4Tb in the NP- Ni_4Tb hybrid. The shape of the XAS and XMCD data at Tb and Ni edges is very similar in the hybrid NP- Ni_4Tb and the pure Ni_4Tb complex. This is a clear indication that the complex has been linked to the NP without suffering major modifications to its structure and the coupling between Ni and Tb is still ferromagnetic. In order to understand the Fe XMCD signal, the

nature of the iron oxide NP must be considered. The NP is formed by a solid solution of both Fe_2O_3 and Fe_3O_4 , so there are defects in the structure to ensure charge balance. The Fe XMCD signal is the combination of hexacoordinated Fe(II) and hexacoordinated and tetraordinated Fe(III) that are antiferromagnetically coupled. The calculated magnetization using the sign of the maximum XMCD L_3 and M_5 edge of Ni and Tb is opposite to that of the 709 eV L_3 band for the tetrahedral Fe(III) ions and parallel to the Fe(II) and Fe(III) hexacoordinated Fe centers in the magnetic nanoparticle. The magnetization data collected do not allow us to affirm that the SMM Ni_4Tb is indeed coupled to the iron oxide NP. The bulk SQUID data at 2 K suggests a weak coupling but the XMCD data obtained at approx. 7 K at the sample are not conclusive. The XMCD measured at Fe edge at 3 T is 25% smaller than the XMCD measured at -3 T, this suggests that some Fe spins are not following the magnetic field. The expectation values calculated for Ni and Tb in the NP- Ni_4Tb system are reduced from the values of the pure compound: $m_z = 0.45 \mu_B$ for Ni and $m_z = 1.74 \mu_B$ for Tb, clear indication that not all spins are following the magnetic field. At all fields studied the moments of tetraordinated Fe(III) in the iron oxide are antiparallel to hexacoordinated Fe(III) and hexacoordinated Fe(II), and to Ni/Tb of Ni_4Tb .

Experimental Section

All chemicals and solvents were purchased from commercial sources and used as received. Microwave assisted reactions were performed in a CEM Discover microwave reactor. Chp stands for deprotonated 6-chloro-2-hydroxypyridine ($\text{C}_5\text{H}_3\text{ClNO}$). tBu-SALOH stands for monodeprotonated 3,5-ditertbutylsalicylic acid ($\text{C}_{15}\text{H}_{21}\text{O}_3$).

$[\text{Ni}_4\text{Tb}(\text{OH})_2(\text{chp})_4(\text{tBuSALOH})_5(\text{H}_2\text{O})(\text{MeCN})(\text{MeOH})]$ (**Ni₄Tb**): Freshly prepared $[\text{Ni}(\text{OH})_2]$ (100 mg, 1.088 mmol), 6-chloro-2-hydroxypyridine (140.94 mg, 1.088 mmol), Tb(III) acetate (91.42 mg, 0.272 mmol) and 3,5-ditertbutylsalicylic acid (338.84 mg, 1.36 mmol) were finely ground and placed in a microwave reactor. A 300 W microwave pulse was applied for 10 minutes at 170 °C. The resulting solid was dissolved in the minimum quantity of MeOH/MeCN (1:1) and then filtered warm obtaining a green solution. Green crystals grew in circa 20 days. Ni_4Tb was characterized using single crystal X-Ray Diffraction, IR, EA and SQUID magnetometry. Yield: 138 mg (22%). Calculated Elemental Analysis for $\text{C}_{106}\text{H}_{143}\text{Cl}_5\text{N}_6\text{Ni}_4\text{O}_{27}\text{Tb}$: C, 50.9%; N, 3.3%; H, 5.7%. Found Elemental Analysis: C, 50.9%; N, 3.3%; H, 5.6%. IR data (KBr, cm^{-1}): 2958 (s), 2869 (m), 2362 (w), 2339 (w), 1653 (w), 1593 (s), 1558 (s), 1445 (s), 1392 (s), 1360 (m), 1244 (m), 1172 (w), 943 (w), 815 (m), 796 (m), 724 (w).

$[\text{Ni}_4\text{La}(\text{OH})_2(\text{chp})_4(\text{tBuSALOH})_5(\text{H}_2\text{O})_{1.5}(\text{MeOH})_{1.5}]$ (**Ni₄La**): Ni_4La was prepared following the same procedure as for Ni_4Tb using La(III) acetate (85.96 mg, 0.272 mmol) instead of Tb(III) acetate. Yield: 41 mg (7%). Calculated Elemental Analysis for $\text{C}_{110}\text{H}_{146}\text{Cl}_6\text{N}_7\text{Ni}_4\text{O}_{29}\text{La}$: C, 50.5%; N, 3.7%; H, 5.6%. Found Elemental Analysis: C, 50.4%; N, 3.5%; H, 5.4%. IR data (KBr, cm^{-1}): 2958 (s), 2870 (m), 2361 (w), 2339 (w), 1653 (m), 1593

(s), 1558 (s), 1444 (s), 1392 (s), 1361 (m), 1295 (w), 1244 (m), 1202 (w), 1162 (m), 992 (m), 927 (m), 815 (m), 794 (m), 725 (m).

NP- Ni_4Tb : Synthesis of the NPs using iron (II) and iron (III) sulfates as precursors was carried out using the method described in the literature.¹⁷ Functionalization with dopamine was carried out using a variation of the method described in the literature.¹⁸ 250 mg of NPs, 250 mg (1.318 mmol) of dopamine and 10 ml of MeOH were refluxed for 4 hours at 55°C using porcelain instead of a magnetic stirrer. The NP-dop are separated magnetically and re-dispersed in MeOH. NP-dop Found Elemental Analysis: C, 4.50%; N, 0.58%, H, 0.66%. The final solution was divided in three parts that were treated the same way. 10 mg (0.0044 mmol) of Ni_4Tb were added to one part and shaken overnight to obtain the surface modified NP. The NP- Ni_4Tb hybrid material is separated magnetically and washed. The **NP- Ni_4Tb** can be re-dispersed in MeOH.

X-Ray diffraction data were collected on a Bruker APEXII SMART diffractometer using Molybdenum $K\alpha$ microfocus ($\lambda=0.71073\text{\AA}$) radiation source. Cif files can be obtained free of charge from the Cambridge Structural Database (<http://www.ccdc.cam.ac.uk/>, deposition numbers 1455786 and 1455787). Magnetic measurements, Dynamic Light Scattering (DLS) and Transmission Electron Microscopy were performed at the CCiT of the Universitat de Barcelona. X-Ray Magnetic Circular Dichroism spectra were measured at the soft X-ray ID32 beamline at ESRF, Grenoble.⁵³ Low temperature hysteresis measurements were performed with an array of micro-SQUIDs at CNRS. Further experimental details can be found in the Supplementary Information.

Conclusions

The proposal of using molecular nanomagnets for application like information processing, spintronics or information storage remains a challenging goal towards which others and we want to contribute. Very relevant to this goal is the possibility to graft or deposit molecular nanomagnets or SMMs intact on a substrate and to be able to show that the molecular species retain their properties while on the surface. This substrate can be a conducting surface like that of an electrode or a magnetic surface. We believe a good model system is nanoparticles, magnetic or metallic, that can be decorated with a molecular species. In this paper we used a heterometallic 3d-4f complex and iron oxide nanoparticles. Heterometallic complexes Ni_4Tb and Ni_4La were obtained by a new microwave assisted solvent-free synthesis method. We have proved that nanostructured hybrid materials composed of iron oxide nanoparticles and high nuclearity coordination complexes can be obtained. The XMCD studies performed show without ambiguity that the heterometallic Ni_4Tb complex is intact on the surface of the NP. Furthermore, the SQUID and XMCD data support a ferromagnetic coupling between Ni and Tb in Ni_4Tb and that this is maintained intact on the hybrid Ni_4Tb -NP system, retaining its magnetic properties. This opens up great possibilities in nanostructured materials of molecular systems,

since it should be now possible to effectively control coupling or to decouple the SMM from the substrate and thus observe the inherent bistability of SMMs on a surface.

Acknowledgements

ECS, GA and LRP acknowledge the financial support from the Spanish Government, (Grants CTQ2012-32247, CTQ2015-68370-P). YL and WW acknowledge the EU for financial support within the FP7 FET-Proactive project MoQuaS N. 610449 and for the Agence Nationale de la Recherche (France) for project MolQuSpin, N. ANR-13-BS10

Notes and references

- J. Camarero, E. Coronado, and A. Epstein, *J. Mater. Chem.*, 2009, **19**, 1678–1684.
- L. Bogani and W. Wernsdorfer, *Nat. Mater.*, 2008, **7**, 179–186.
- S. Sanvito and A. R. Rocha, 2006.
- J. Lehmann, A. Gaita-Ariño, E. Coronado, and D. Loss, *J. Mater. Chem.*, 2009, **19**, 1672.
- D. Stepanenko, M. Trif, and D. Loss, *Inorganica Chim. Acta*, 2008, **361**, 3740–3745.
- M. N. Leuenberger and D. Loss, *Nature*, 2001, **410**, 789–793.
- F. Meier, J. Levy, and D. Loss, *Phys. Rev. Lett.*, 2003, **90**, 047901.
- P. Tyagi, *J. Mater. Chem.*, 2011, **21**, 4733.
- F. Prins, A. Barreiro, J. W. Ruitenber, J. S. Seldenthuis, N. Aliaga-Alcalde, L. M. K. Vandersypen, and H. S. J. van der Zant, *Nano Lett.*, 2011, **11**, 4607–4611.
- H. B. Heersche, Z. De Groot, J. A. Folk, H. S. J. Van Der Zant, C. Romeike, M. R. Wegewijs, L. Zobbi, D. Barreca, E. Tondello, and A. Cornia, *Phys. Rev. Lett.*, 2006, **96**, 1–5.
- L. M. Bronstein, X. Huang, J. Retrum, A. Schmucker, M. Pink, B. D. Stein, and B. Dragnea, *Chem. Mater.*, 2007, **19**, 3624–3632.
- J. Park, K. An, Y. Hwang, J. Park, H. Noh, J. Kim, J. Park, N. Hwang, and T. Hyeon, *Nat. Mater.*, 2004, **3**, 891–895.
- A. Lu, E. L. Salabas, and F. Schüth, *Angew. Chemie, Int. Ed.*, 2007, **46**, 1222–1244.
- M. Colombo, S. Carregal-Romero, M. F. Casula, L. Gutiérrez, M. P. Morales, I. B. Böhm, J. T. Heverhagen, D. Prospero, and W. J. Parak, *Chem. Soc. Rev.*, 2012, **41**, 4306.
- W. Lin, *Chem. Rev.*, 2015, **115**, 10407–10409.
- S. H. Gage, B. D. Stein, L. Z. Nikoshvili, V. G. Matveeva, M. G. Sulman, E. M. Sulman, D. G. Morgan, E. Y. Yuzik-Klimova, W. E. Mahmoud, and L. M. Bronstein, *Langmuir*, 2013, **29**, 466–473.
- V. Polshettiwar and R. S. Varma, *Chem. - A Eur. J.*, 2009, **15**, 1582–1586.
- D. Guin, B. Baruwati, and S. V. Manorama, *Org. Lett.*, 2007, **9**, 1419–1421.
- M. Mannini, F. Pineider, P. Sainctavit, C. Danieli, E. Otero, C. Sciancalepore, A. M. Talarico, M.-A. Arrio, A. Cornia, D. Gatteschi, and R. Sessoli, *Nat. Mater.*, 2009, **8**, 194–197.
- M. Gonidec, R. Biagi, V. Corradini, F. Moro, V. De Renzi, U. Pennino, D. Summa, L. Muccioli, C. Zannoni, D. B. Amabilino, and J. Veciana, *J. Am. Chem. Soc.*, 2011, **133**, 6603–6612.
- C. Wäckerlin, F. Donati, A. Singha, R. Baltic, S. Rusponi, K. Diller, F. Patthey, M. Pivetta, Y. Lan, S. Klyatskaya, M. Ruben, H. Brune, and J. Dreiser, 2016, 5195–5199.
- C. J. Milios, A. Vinslava, a G. Whittaker, S. Parsons, W. Wernsdorfer, G. Christou, S. P. Perlepes, and E. K. Brechin, *Inorg. Chem.*, 2006, **45**, 5272–4.
- I. a Gass, C. J. Milios, a G. Whittaker, F. P. a Fabiani, S. Parsons, M. Murrie, S. P. Perlepes, and E. K. Brechin, *Inorg. Chem.*, 2006, **45**, 5281–3.
- A. Pons-Balagué, M. J. Heras Ojea, M. Ledezma-Gairaud, D. Reta Mañeru, S. J. Teat, J. Sánchez, G. Aromí, and E. C. Sañudo, *Polyhedron*, 2013, **52**, 781–787.
- M. Ledezma-Gairaud, L. W. Pineda, G. Aromí, and E. C. Sañudo, *Polyhedron*, 2013, **64**, 45–51.
- A. Pons-Balagué, N. Ioanidis, W. Wernsdorfer, A. Yamaguchi, and E. C. Sañudo, *Dalt. Trans.*, 2011, **40**, 11765–11769.
- R. H. Laye, M. Murrie, S. Ochsenein, A. R. Bell, S. J. Teat, J. Raftery, H.-U. Güdel, and E. J. L. McInnes, *Chem. - A Eur. J.*, 2003, **9**, 6215–20.
- E. C. Sañudo, M. Font-Bardia, X. Solans, and R. H. Laye, *New J. Chem.*, 2011, **35**, 842–848.
- E. C. Sañudo, J. Ribas, and R. E. P. Winpenny, *New J. Chem.*, 2007, **31**, 1421–1423.
- J. Dreiser, K. S. Pedersen, C. Piamonteze, S. Rusponi, Z. Salman, M. E. Ali, M. Schau-Magnussen, C. A. Thuesen, S. Piligkos, H. Weihe, H. Mutka, O. Waldmann, P. Oppeneier, J. Bendix, F. Nolting, and H. Brune, *Chem. Sci.*, 2012, **3**, 1024–1032.
- M. Mannini, P. Sainctavit, R. Sessoli, C. Cartier dit Moulin, F. Pineider, M.-A. Arrio, A. Cornia, and D. Gatteschi, *Chem. Eur. J.*, 2008, **14**, 7530–7535.
- L. Malavolti, V. Lanzilotto, S. Ninova, L. Poggini, I. Cimatti, B. Cortigiani, L. Margheriti, D. Chiappe, E. Otero, P. Sainctavit, F. Totti, A. Cornia, M. Mannini, and R. Sessoli, *Nano Lett.*, 2015, **15**, 535–541.
- M. Mannini, F. Pineider, C. Danieli, F. Totti, L. Sorace, P. Sainctavit, M. Arrio, E. Otero, L. Joly, J. C. Cezar, A. Cornia, and R. Sessoli, *Nature*, 2010, **468**, 417–421.
- J. Dreiser, G. E. Pacchioni, F. Donati, L. Gragnaniello, A. Cavallin, K. S. Pedersen, J. Bendix, B. Delley, M. Pivetta, S. Rusponi, and H. Brune, *ACS Nano*, 2016, **10**, 2887–2892.
- M. J. Heras-Ojea, D. R. Mañeru, L. Rosado, J. R. Zuazo, G. R. Castro, S. Tewary, G. Rajaraman, G. Aromí, E. Jiménez, and E. C. Sañudo, *Chem. Eur. J.*, 2014, **20**, 10439–45.
- E. C. Sañudo and L. Rosado Piquer, *Dalt. Trans.*, 2015, **44**, 8771–8780.
- L. Rosado Piquer and E. C. Sañudo, *Dalt. Trans.*, 2015, **44**, 8771–8780.
- S. Das, S. Hossain, A. Dey, S. Biswas, E. Pardo, F. Lloret, and V. Chandrasekhar, *Eur. J. Inorg. Chem.*, 2014, 3393–3400.
- M. A. Halcrow, J. Sun, J. C. Huffman, and G. Christou, *Inorg.*

- Chem.*, 1995, **4**, 4167–4177.
40. N. F. Chilton, R. P. Anderson, L. D. Turner, A. Soncini, and K. S. Murray, *J. Comput. Chem.*, 2013, **34**, 1164–1175.
41. J. Echeverría, G. Aullón, D. Danovich, S. Shaik, and S. Alvarez, *Nat. Chem.*, 2011, **3**, 323–330.
42. S. M. Suturin, V. V. Fedorov, a G. Banshchikov, D. a Baranov, K. V. Koshmak, P. Torelli, J. Fujii, G. Panaccione, K. Amemiya, M. Sakamaki, T. Nakamura, M. Tabuchi, L. Pasquali, and N. S. Sokolov, *J. Phys. Condens. Matter*, 2013, **25**, 046002.
43. M. Estrader, A. López-Ortega, S. Estradé, I. V. Golosovsky, G. Salazar-Alvarez, M. Vasilakaki, K. N. Trohidou, M. Varela, D. C. Stanley, M. Sinko, M. J. Pechan, D. J. Keavney, F. Peiró, S. Suriñach, M. D. Baró, and J. Nogués, *Nat. Commun.*, 2013, **4**, 2960.
44. A. Lodi Rizzini, C. Krull, T. Balashov, J. J. Kavich, A. Mugarza, P. S. Miedema, P. K. Thakur, V. Sessi, S. Klyatskaya, M. Ruben, S. Stepanow, and P. Gambardella, *Phys. Rev. Lett.*, 2011, **107**, 177205.
45. W. Wernsdorfer, N. Aliaga-Alcalde, D. N. Hendrickson, and G. Christou, *Nature*, 2002, **416**, 406–9.
46. T. N. Nguyen, W. Wernsdorfer, K. a Abboud, and G. Christou, *J. Am. Chem. Soc.*, 2011, **133**, 20688–20691.
47. A. L. Rizzini, C. Krull, T. Balashov, A. Mugarza, C. Nistor, F. Yakhou, V. Sessi, S. Klyatskaya, M. Ruben, S. Stepanow, and P. Gambardella, *Nano Lett.*, 2012, 5703–5707.
48. C. Nistor, C. Krull, A. Mugarza, S. Stepanow, C. Stamm, M. Soares, S. Klyatskaya, M. Ruben, and P. Gambardella, *Phys. Rev. B*, 2015, **92**, 184402.
49. C. T. Chen, Y. U. Idzerda, H. J. Lin, G. Meigs, A. Chaiken, G. A. Prinz, and G. H. Ho, *Phys. Rev. B*, 1993, **48**, 642–645.
50. M. Gruber, F. Ibrahim, S. Boukari, H. Isshiki, L. Joly, M. Peter, M. Studniarek, V. Da Costa, H. Jabbar, V. Davesne, U. Halisdemir, J. Chen, J. Arabski, E. Otero, F. Choueikani, K. Chen, P. Ohresser, W. Wulfhekel, F. Scheurer, W. Weber, M. Alouani, E. Beaurepaire, and M. Bowen, *Nat. Mater.*, 2015, **14**, 981–4.
51. V. Cuartero, S. Lafuerza, G. Subias, J. Garcia, E. Schierle, J. Blasco, and J. Herrero-Albillos, *Phys. Rev. B*, 2015, **91**, 1–8.
52. P. Carra, B. T. Thole, M. Altarelli, and X. Wang, *Phys. Rev. Lett.*, 1993, **70**, 694–697.
53. K. Kummer, A. Fondacaro, E. Jimenez, E. Velez-Fort, A. Amorese, M. Apsbury, F. Yakhou-Harris, P. van der Linden, and N. B. Brookes, *J. Synchrotron Radiat.*, 2016, **23**, 1–4.